Hysterons and pathways in mechanical metamaterials

Ding, J.

CHAPTER 5

PATTERN FORMATION, FRUSTRATION, AND THE FIRST UNSTABLE MODE OF A MONOHOLAR MECHANICAL METAMATERIAL

5.1 Introduction

The onset of pattern formation in monoholar metamaterials, slabs patterned with a square array of equal sized holes, is due to a collective buckling of the vertical, symmetric beam like structures in these materials. One finds that under compression the holes in the metamaterial form a pattern of alternating horizontal and vertical ellipses [2, 3, 11, 30, 34–39]. Despite having been studied extensively, one mystery has remained: A priory, two symmetry-related patterns ('A' and 'B') could form — how does the sample select which pattern is created? Numerically, tracking symmetry breaking buckling instabilities is not trivial, and often one weakly breaks the symmetry to avoid such problems, yielding homogeneous patterns [34, 70]. Experimentally, one finds that any given sample is typically sufficiently symmetry broken so that always the same pattern is formed — where it may be that plastic deformations due to repeated compression cycles

'train' the material to have a certain mode. However, in large samples (say 20×20 holes), one finds that domain walls form between patches of patterns A and B. In addition, the force-compression curves of monoholar samples occasionally show a peak near the onset of pattern formation, but the presence of this peak seems to poorly reproduce.

In this chapter we investigate the onset of patterning in monoholar samples. We simulated the compression process of the holey metamaterial via Abaqus/standard (Section A.4). We define mode A and mode B as follows: In mode A, all the x-polarized (y-polarized) holes (i, j) have $i + j = 2, 4, 6,$ ... $(1, 3, 5, ...)$; in mode B, all the x-polarized (y-polarized) holes (i, j) have $i + j = 1, 3, 5, ...$ $(2, 4, 6, ...)$.

We first investigate the first unstable mode in numerical simulations of perfectly symmetric samples, and we find that, depending on the parity (odd or even) of the number of columns or rows of holes, the pattern can split up into two or even four patches — these reflect the symmetry of the sample, but lead to frustration. We then show that such frustrated patterns can relax into single-patch patterns, both in simulations and in experiments, and that such a switch from a frustrated to the simple pattern is associated with a sudden drop in the compressive force — suggesting that such frustrations play a role in the mechanics of monoholar samples. Finally we explore using defects — single holes of different size that break the symmetries of the undeformed sample and depending on location favor mode A or mode B — can be used to further manipulate the response.

5.2 Phenomenology

We perform 2D plane strain (CPD4R) Abaqus simulations of monoholar samples made of a Neo-Hookean material. We fix P = 5 mm, take samples without lateral walls, and focus on samples with hole diameter $D = 4$ mm. In particular we study the effect of even and odd rows and columns of holes in $m \times n$ samples, for $m \times n = 9 \times 9, 9 \times 10, 10 \times 9$ and 10×10.

To motivate our studies, we show in Fig. 5.1 the patterns that form. First, we notice that all patterns are spatially heterogeneous — near the fixed top and bottom boundary, the pattern is suppressed, and near the lateral boundaries, the patterns tends to be amplified. Surprisingly, while the pattern for the 9×9 sample consist of a single patch of mode A, for the other samples the pattern breaks up into two patches (9×10 and 10×9 samples) or even in four patches (10×10 sample).

The stress-strain curves of these four samples are shown in Fig. 5.2. We note that the while the pre-buckling slopes are very similar, the post-buckling slopes are significantly different, with the 9×9 and 9×10 having a significant negative slope, while the 10×9 and 10×10 samples have a flatter post-buckling response. At the same time, we observe that the samples with 9 rows buckles earlier than the samples with 10 rows.

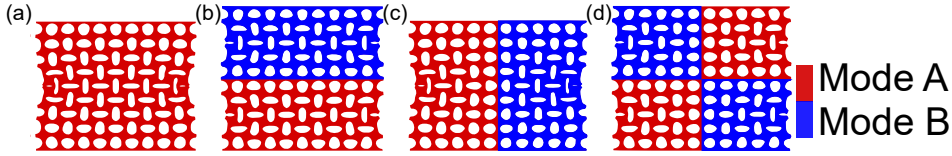

FIGURE 5.1: The simulation result of the first mode in the biholey metamaterial. P = 5 mm, D = 4.0 mm, ε = 0.1. The sample has (a) 9×9, (b) 9×10, (c) 10×9, or (d) 10×10 holes.

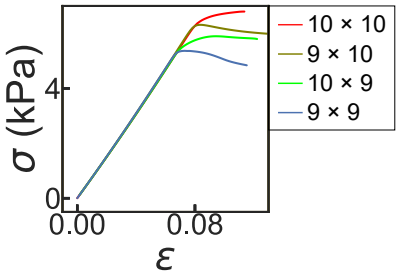

FIGURE 5.2: Stress-strain response of the sample shown in Fig. 5.1.

The results strongly suggest that competition between the different symmetry related modes A and B could play a role in modifying and selecting the observed patterns, as well as at the mechanical response. A more precise analysis requires to follow the evolution of these patterns quantitatively, and we develop techniques and order parameters to do so in the following sections.

5.3 Numeric procedure: Pattern tracking and flattening

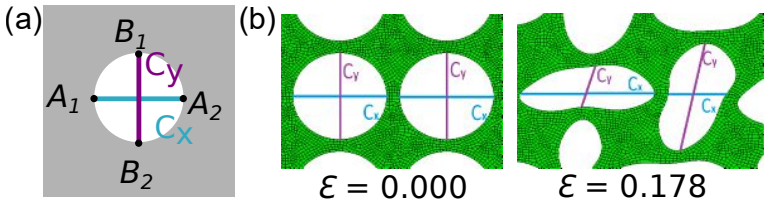

FIGURE 5.3: (a) Sketch of the holes and nodes. The gray region is the sample. A_1, A_2, B_1 and B_2 are the names for the nodes. C_x and C_y denote the line between A_1 and A_2 or B_1 and B_2. (b) An example of a part of the sample before and after compressing, which includes a x-polarized and a y-polarized hole. Axes C_x and C_y are labeled in the figure. For details, see text.

The polarization of the hole is recorded by tracking the long and short axes of the holes when the sample is compressed. Now we describe the process of tracking the polarization in the Abaqus simulation. We track the polarization by tracking the top, bottom, left, and right nodes of the hole. To do so, we set 4 special nodes on the boundary line of the hole, as shown in Fig. 5.3 (a). It is much easier for Abaqus to track an independent reference point than a node on the numerical sample, so we build four 2D reference points A_1, A_2, B_1 and B_2. In Abaqus, the reference points can be named by the hole's name and the node's name, such as *'hole_i_j − node_A_1'*. Then we use the history output to output the coordinate of all the reference

points and save it to a CSV file. The frequency of collecting data is 0.01 units of time.

The long and the short axes of the elliptical holes are:

$$C_x = \sqrt{(x_{A1} - x_{A2})^2 + (y_{A1} - y_{A2})^2)} \tag{5.1}$$

$$C_y = \sqrt{(x_{B1} - x_{B2})^2 + (y_{B1} - y_{B2})^2)} \tag{5.2}$$

Geometrically, not all the holes are ellipses when the sample is compressed. Even though the shape of the hole is a complex shape similar to an ellipse, by observing the system, we found that the lengths of C_x and C_y help us distinguish the polarization of the holes and the character of the pattern domain, as shown in Fig. 5.3 (b). In this aspect, we use the order parameter F_h for the flattening [2, 3, 11, 30, 34–39] of hole:

$$F_h = \frac{C_x - C_y}{C_x + C_y} \tag{5.3}$$

Even though the long axes of the elliptical hole are not always in the x- or y-direction, by comparing adjacent holes, we divide the holes into near holes x-polarized and nearly y-polarized holes, such as the left and right holes shown in Fig. 5.3 (b), where x-polarized (y-polarized) hole correspond to $F_h > 0$ ($F_h < 0$).

5.4 The First Unstable Mode in Monoholar Samples

As shown in Section 1.3, the holes in monoholar samples deform to horizontal and vertical ellipses under compression. To investigate this process and the associated patterning instability, we perform 2D plane strain (CPD4R) Abaqus simulations of monoholar samples made of a Neo-Hookean material. We fix P = 5 mm, take samples without lateral walls, and focus

on samples with hole diameter $D = 4$ mm. In particular we study the effect of even and odd rows and columns of holes in $m \times n$ samples, for $m \times n = 9 \times 9, 9 \times 10, 10 \times 9$ and 10×10.

We characterize the sample deformations by the stress-strain response, as well as by the spatial patterns of modes A and B, which we detect by studying the shape changes of each hole as function of the strain. We first discuss how to distinguish a global "flattening" of the holes due to vertical compression to the alternating hole patterns due to the collective buckling instability, focussing on a 9×9 sample, and then use these techniques to study the other sample sizes as well.

5.4.1 Order parameters: 9×9 sample

The stress-strain response (Fig. 5.2a) shows a nearly linear increase of the stress for $\varepsilon < 0.064$, a kink, and then a slight decrease of the stress for $\varepsilon > 0.064$. The linear increase is associated with the pre-patterning regime, whereas the kink signals the onset of pattern formation [35]. To study this onset of patterning in detail, we track the flattening F_h for all holes as function of strain. Our data shows the onset of the patterning for strains above the critical strains and its subsequent growth (Fig. 5.4(a)). Clearly the signs of F_h of neighboring holes are opposite (Fig. 5.4b), and to obtain a non-staggered measure of the holes polarization, we define:

$$\Omega = (-1)^{i+j} \times F_h \,. \tag{5.4}$$

We show Ω in Fig. 5.4c. Indeed we find that the sign of Ω is the same throughout the pattern. However, we also observe some residual "checkerboard" patterns in Ω, even before the onset of patterning. To understand this, we note that, even without patterning, compression slightly flattens the holes: so its deformations are a mix of uniform compression and staggered pattern formation. To only focus on the patterning, we subtract the mean flattening $< F_h >$ (take over all holes in the sample) and introduce F'_h

and Ω':

$$F'_h = F_h - < F_h > , \tag{5.5}$$

$$\Omega' = (-1)^{i+j} \times (F_h - < F_h >) . \tag{5.6}$$

First, we note that plots of Ω' show the absence of patterning below the threshold, and the smooth growth of the patterning mode above the threshold (Fig. 5.4d). Nevertheless, the mode is not homogeneous, due to boundary effects — the order parameter Ω' is well suited to capture this inhomogeneity. Moreover, Ω' gives a simple measure to distinguish the two possible stable orthogonal patterns, mode-A or mode-B (Section 5.1): $\Omega' < 0$ corresponds to mode A and $\Omega' > 0$ correspond to mode B.

To facilitate a comparison of the spatial inhomogeneity of the modes at different strain, we introduce a normalized order parameter

$$\Omega'_N = \frac{\Omega'}{\sqrt{\sum_{i,j} \Omega'^2}} . \tag{5.7}$$

Plots of Ω'_N below the threshold mainly show noise, but for all plots above the threshold, we immediately see now that the pattern formation is strongest near the lateral edges, and moreover, gets spatially more concentrated for increasing strain (Fig. 5.4e). In other words, the rate of deformation of the holes is spatially dependent. Our order parameters allow to precisely follow how the mode B pattern forms and spreads in a 9 $\times$ 9 sample under compression.

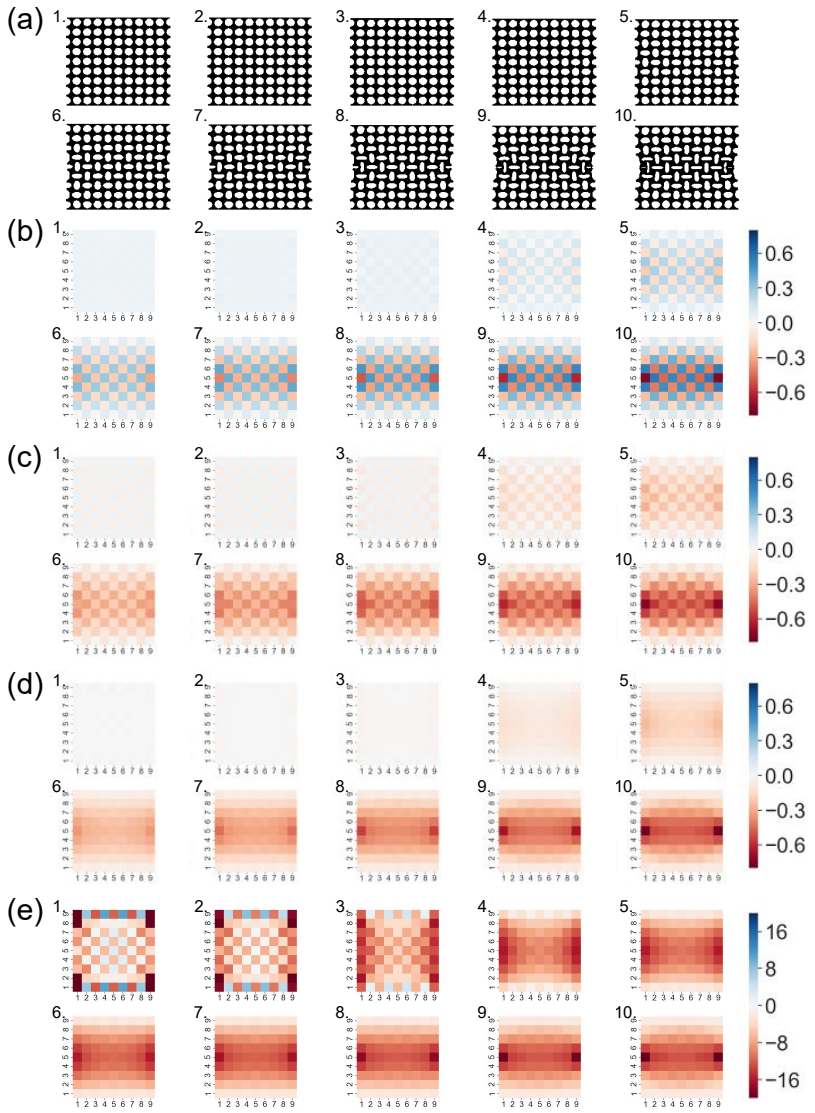

FIGURE 5.4: (a) Snapshots of a compressed 9×9 sample with D = 4.0 mm for ε = 0.0533, 0.0587, 0.0640, 0.0693, 0.0747, 0.0800, 0.0853, 0.0907, 0.0960 and 0.1013. (b) Hole shape F_{lh} of as a function of hole position (i, j) for the same data as shown in panel (a). (c) Staggered order parameter Ω for the same data as shown in panel (a). (d) Staggered and background-compensated order parameter Ω' for the same data as shown in panel (a). (e) Normalized staggered order parameter Ω'_N for the same data as shown in panel (a).

5.4.2 Samples with even number of rows or columns

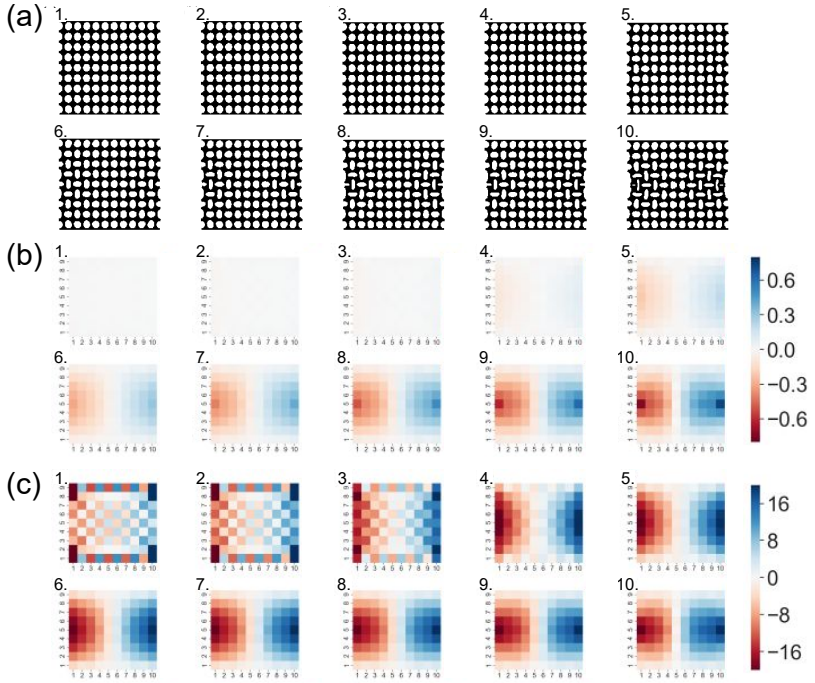

FIGURE 5.5: (a) Snapshots of a compressed 10×9 sample with D = 4.0 mm forε = 0.0533, 0.0587, 0.0640, 0.0693, 0.0747, 0.0800, 0.0853, 0.0907, 0.0960 and 0.1013. (b - c) Corresponding staggered order parameters Ω' and normalized order parameters Ω'_N for these patterns reveals the emergence of two patches of mode A and B respectively.

In this section we discuss the more complex patterns that emerge in samples with an even number of columns or holes, and even number of rows, or both.

We start with a sample of 10×9, where we show the real space snapshots, the staggered order parameter Ω', and the normalized staggered order parameter Ω'_N (Fig. 5.5). As expected, for small compression the hole deformations are relatively homogeneous and small. At the critical strain

$\varepsilon \approx 0.070$, the alternating hole pattern appears, but due to the even number of columns we observe the emergence of two patches, one with mode A and one with mode B. This produces frustration in the middle of the sample, as these two patterns are not compatible. As before, we notice that the pattern is strongest near the edges, and for increasing strain also increasingly gets localized.

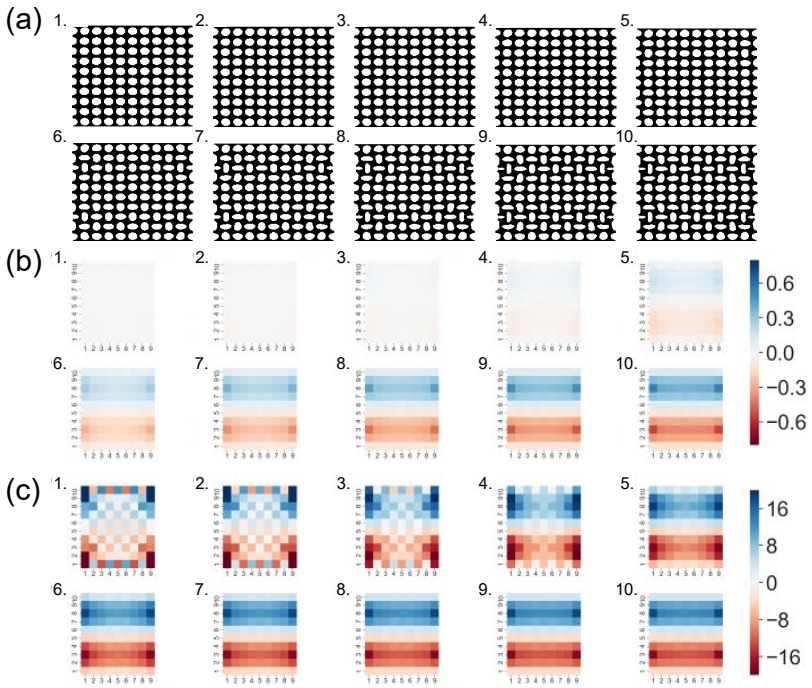

FIGURE 5.6: (a) Snapshots of a compressed 9×10 sample with D = 4.0 mm for $\varepsilon = 0.0624, 0.0672, 0.0720, 0.0768, 0.0816, 0.0864, 0.0912, 0.096, 0.1008$ and 0.1056. (b-c) Corresponding plots of staggered order parameter Ω' and normalized staggered order parameter Ω'_N.

For a sample with an even number of rows, we again find two patches, now stacked on top of each other (Fig. 5.6). Along a horizontal band in the middle, the system is frustrated and the holes, in good approximation, are equally patterned. Again, the patterns are strongest near the lateral edges, although we do not observe increasing localization with increasing strain

— perhaps because even at small strains the concentration is already quite strong.

For a sample with both an even number of rows and columns, the pattern breaks up in four patches. The formation of this ABAB pattern is shown in Fig. 5.7. The frustration between A and B patterns prevents a significant part of the sample to form patterns; this may explain its relatively large stiffness (Fig. 5.2).

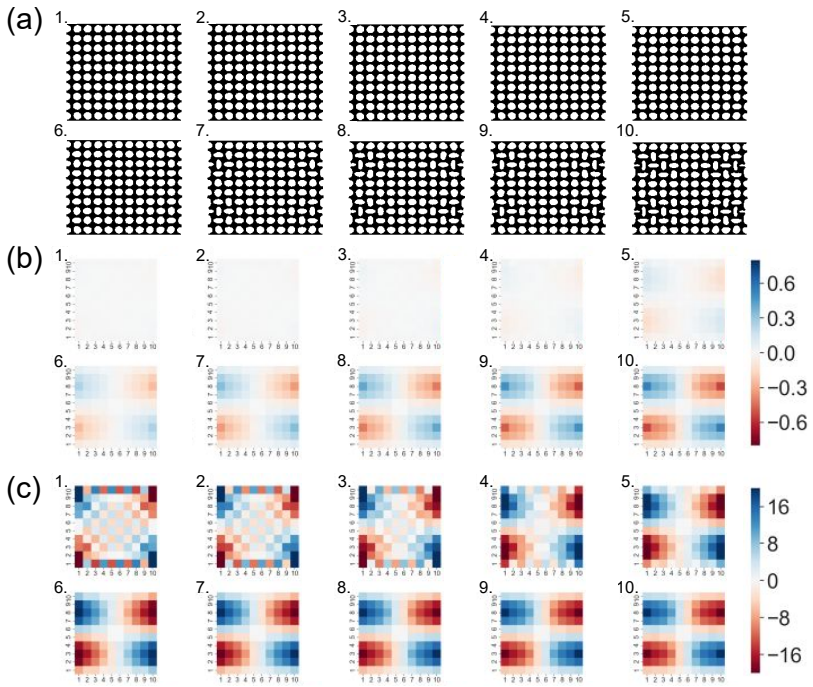

FIGURE 5.7: (a) Pattern evolution in a 10×10 sample for $\varepsilon = 0.0624$, 0.0672, 0.0720, 0.0768, 0.0816, 0.0864, 0.0912, 0.0960, 0.1008 and 0.1056. (b-c) Corresponding staggered order parameter Ω' and normalized order parameter Ω'_N.

Together, our data show the formation of multiple patches of mutually incompatible patterns in homogeneously compressed samples where either the number of columns, number of rows, or both are even. In all cases, the

pattern tends to be strongest near the boundaries. Our results show that while a homogeneous picture of the deformations in monoholar samples is a good starting point for large and 'odd' samples, reflection symmetries may lead to more complex patterns. Moreover, our data suggest that higher degrees of frustration lead to stiffer samples in the post-buckling regime (Fig. 5.2), and impact the mechanical response of these metamaterials [35].

5.5 Scrambling and cooperating of the regimes

5.5.1 Mode competition and defects

In this final section, we explore the competition between deformation modes A and B, and also outline a general defect-based strategy with which we can 'seed' these modes. As we have seen above, not all the holes deform in the same mode. Typically, once a hole becomes polarized, it typically does not change its polarization. However, we present two examples where, in simulations, the system spontaneously switches between two different polarization patterns when the strain is increased. We note that these examples where discovered by accident in large data sets where we systematically varied the hole diameter; in most runs, there is no pattern switch.

First, we consider the polarization pattern for a 9×9 sample with $D = 0.46$ mm. Initially, the sample forms a pattern of three vertical bands of modes B, A and B (B near the edges, A in the middle) (Fig. 5.8a). Further increasing of the stress leads to a sudden switch around $\varepsilon = 0.025$ to a pattern of only mode A (Fig. 5.8b). Associated with this switch is a sudden drop in the force (Fig. 5.8c). We note that, consistent with this, the data shown in the previous section finds the same link between frustration and force, i.e. less frustration leads to lower forces (Fig. 5.2). Finally we have tracked the polarization Ω' as function of strain for 25 holes (i, j both ranging from 1 to

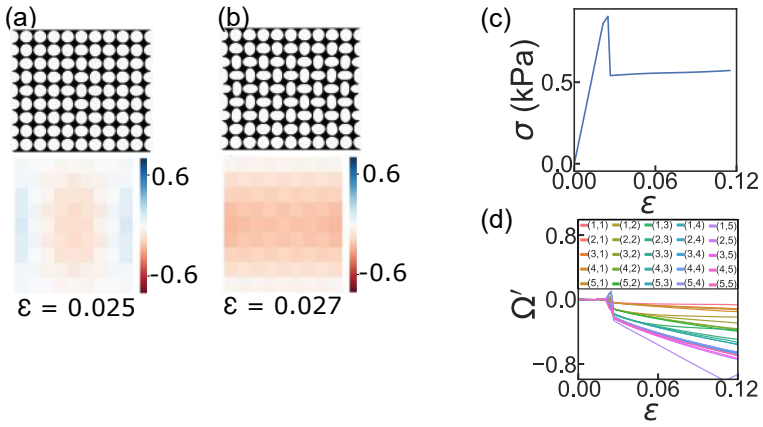

FIGURE 5.8: An example of the holes on columns 1, 2, 8 and 9 snap at $\varepsilon = 0.025$, where $D = 0.46$ mm. (a-b) Snapshot and staggered order parameter Ω' before and after snapping. (c) $\sigma - \varepsilon$ curve shows a sharp drop at $\varepsilon = 0.025$ featuring snapping action. (d) $\Omega' - \varepsilon$ curves show a sharp jump at $\varepsilon = 0.025$.

5). These further show the sharp jump in local polarization at the switching event (Fig. 5.8d)

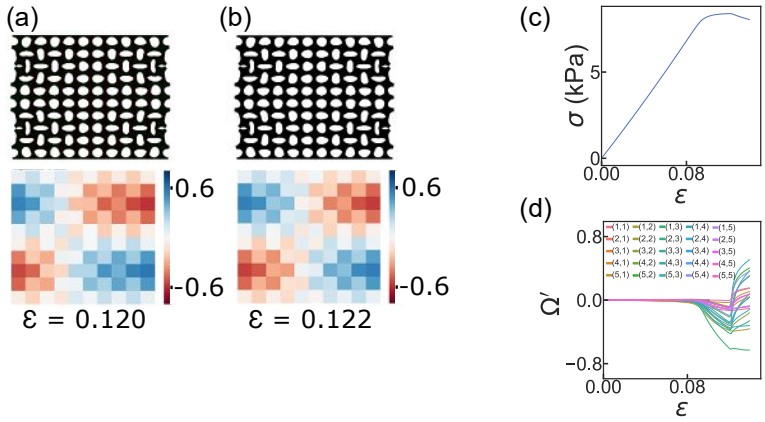

FIGURE 5.9: An example of holes on column 5 snaps at $\varepsilon = 0.120$ where $D = 3.9$ mm. (a-b) Snapshot and staggered order parameter Ω' before and after snapping. (c) $\sigma - \varepsilon$ curve shows a subtle kink at $\varepsilon = 0.120$. (d) $\Omega' - \varepsilon$ curves show a sharp jump at $\varepsilon = 0.120$.

A more subtle switch was observed in a 10×10 sample. These form a pattern of four patches, but we found one example where the location of the vertical domain wall jumped by one column (Fig. 5.9a-b) under a compressive strain of order $\varepsilon = 0.122$. The associated stress-strain curve shows a subtle kink at this switching strain (Fig. 5.9c). Finally, the polarization Ω' as function of strain also evidences this pattern switch (Fig. 5.9d).

We interpret these results as illustrating the sensitivity of the pattern formation process to, in this case, uncontrolled perturbations that break the initial symmetry and lead to the formation of either mode A or B patterns. We suggest that rationally design symmetry breaking perturbations could be used to control the evolution of these modes.

5.5.2 Defects

We close this thesis with a short exploration of the role of defects in monoholar patterns. Based in the symmetry breaking used in biholar samples, the central idea is to embed one or two larger (or smaller) holes in a regular monoholar pattern to break the symmetry, and to locally seed mode A or mode B. We focus on experiments.

We first compare four samples with the same monoholar pattern with $D = 3.9$ mm — specifically, a pattern without a defect (Fig. 5.10a*i*), a pattern where one hole is filled - or replaced with a defect hole of diameter $D_d = 0$ mm (Fig. 5.10a*ii*), a pattern with one smaller hole ($D_d = 3.0$ mm, (Fig. 5.10a*iii*) and a pattern with one larger defect hole of diameter $D_d = 5.0$ mm (Fig. 5.10a*iv*). In all cases the holes are placed such that they are compatible with mode A. We note that the smaller defect holes do not impact the pattern formation or mechanical response significantly (Fig. 5.10b). In contrast, the larger defect hole already seeds a mode A pattern for strains below the critical strain (0.12), as seen in the second panel of (Fig. 5.10a*iv*). As a result, the peak values of the stress are lower and shifted leftward — hence a larger defect hole suppresses the instability.

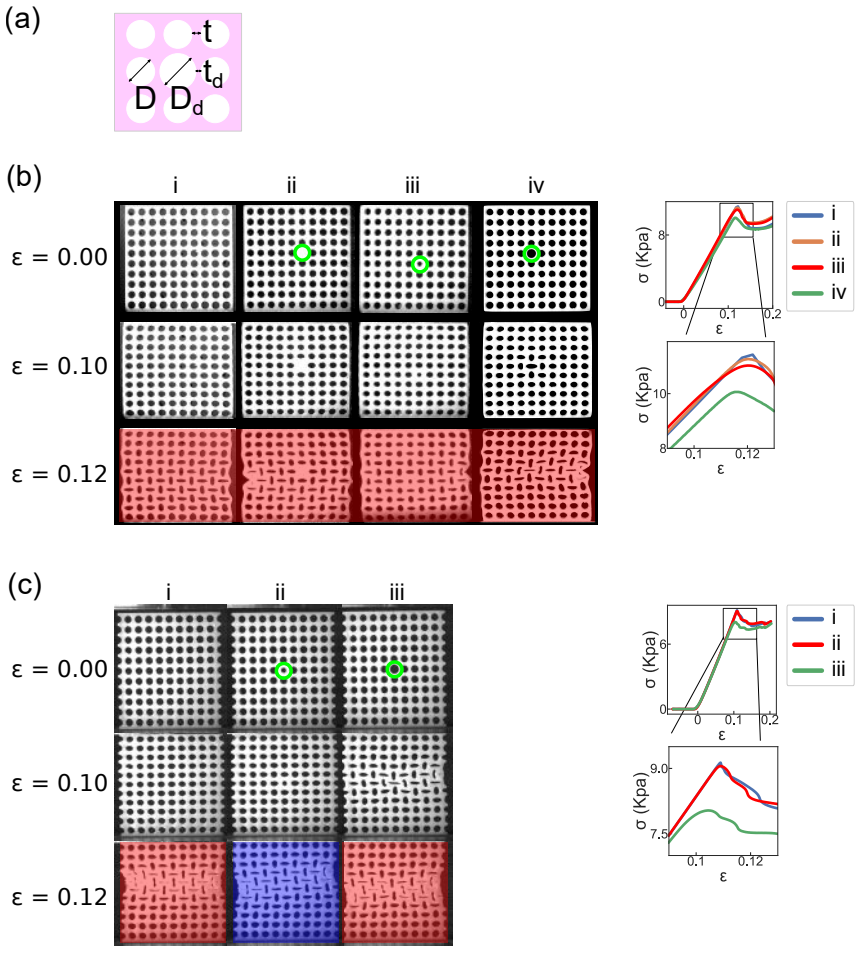

FIGURE 5.10: A defect hole can break the symmetry and seed modes of holey metamaterial. The defect holes are heightened by green cycles. Mode A (mode B) is highlighted in red (blue) when $\varepsilon = 0.12$. The samples have $\{P, D, t_x, t_y\} = \{5$ mm, 3.9 mm, 0.5 mm, 0.5 mm $\}$. (a) Sketches of the holey sample with a defect hole with diameter D_d. (b) Evolution of the sample with side walls (left) and the $\sigma - \varepsilon$ response (right) showing buckles earlier than the monoholar sample. The samples are characterized with (i) monoholar pattern, (ii) a pattern with one replaced defect ($D_d = 0$ mm), (iii) a pattern with one smaller hole ($D_d = 3.0$ mm), and (iv) a pattern with one larger hole ($D_d = 5.0$ mm). (c) Sample without side walls. The samples are charactered with (i) monoholar pattern, (ii) a pattern with one smaller hole ($D_d = 3.0$ mm), and (iii) a pattern with one larger hole ($D_d = 5.0$ mm).

The data shown in Fig. 5.10c shows two things. First, using a smaller or larger defect at the same location, the defect can seed either mode A or mode B — once the pattern starts to develop around the defect, which is already visible at strain 0.1, slightly below the peak strain of 0.11, this pattern spreads out throughout the whole sample. Second, while a smaller defect hole does not impact the mechanical stiffness, a larger defect hole again suppresses the instability and leads to a significantly smaller peak stress (Fig. 5.10c, right).

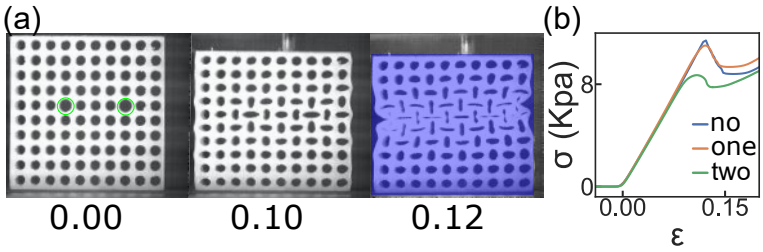

FIGURE 5.11: A pair of commensurate defects further suppresses the instability of the holey metamaterial, where the sample has $\{P, D, D_d\}$ = {5 mm, 3.9 mm, 5 mm }. (a) Evolution of the sample. The defects are heightened by the green cycles. Mode A (mode B) observed at $\varepsilon = 0.10$ is highlighted in red (blue). (b) $\sigma - \varepsilon$ response. Compared to the monoholar sample (blue curve) and the sample with one defect hole (orange curve), which snapshots are shown in Fig. 5.10b, the sharp peak is further smeared out by a pair of defect holes.

In Fig. 5.11 we show the effect of two defect holes that are placed at a distance of four holes, i.e., which are commensurate, as they seed the same mode. While the formation of patterns does not show any significant change due to these defects, again the peak stress is lowered, and the sharp transition seen in the absence of defects, and smeared out in the presence of a single defect, is even further smeared out and suppressed by this pair of defects (Fig. 5.11b).

Finally, we have also explored the effect of placing two defect nodes at incommensurate positions, so that they seed different modes (Fig. 5.12). When placed close together, we find that quickly one of the patterns takes over, and for larger compression we find a single deformation mode (Fig. 5.12a). This is reminiscent of the quick pattern switching that we also observed in numerical simulations above. In contrast, for two incom-

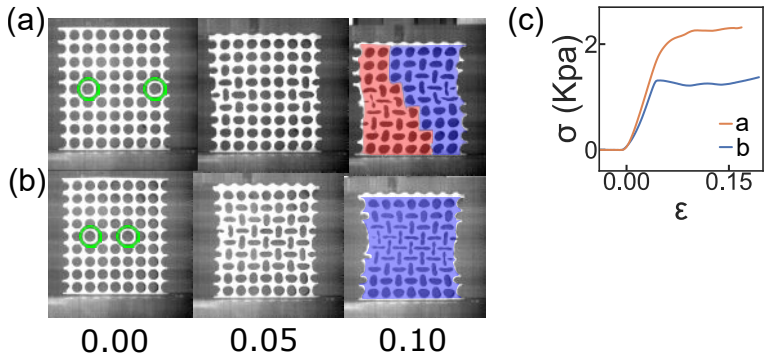

FIGURE 5.12: A pair of incommensurate defects can either trigger one pattern or two different patterns; here the samples have $\{P, D, D_d\}$ = {5 mm, 4.4 mm, 5 mm }. The defects are highlighted by the green cycles. Mode A (mode B) is highlighted in red (blue). (a) Under compression, one mode is observed in the sample with two defect holes that are placed at a distance of five holes. (b) Under compression, two modes are observed in the sample with two defect holes that are placed at a distance of three holes. (c) $\sigma - \varepsilon$ curves showing the domain wall between different modes stiffen the sample.

mensurate defects placed further apart, the sample exhibits both mode A and B, even at large post-buckling strain (Fig. 5.12b). In that case, the sharp kink in the stress curves is smeared out, and the post-buckling stress is much higher than for the single domain sample (Fig. 5.12c), again showing that domain walls significantly stiffen the sample.

Together, our exploratory experiments indicate the utility of defect holes. Single defect holes can be used to control the mode of the sample, and larger defect holes can smear out the pattern forming instability and lower the post-buckling stiffness. Pairs of defects can be used to seed multiple patterns and domain walls, which significantly stiffen the sample in the post-buckling regime. Many open questions remain: How far can a single defect seed a pattern? What is the minimal distance for pairs of defects to generate multiple domains? Can we use other defects (for examples holes shifted from their grid position) to seed even more complex patterns? It is however clear that defects can play a crucial role in controlling and modifying the pattern forming instabilities for the well-studied monoholar metamaterials.

5.6 Conclusion

In this chapter, we have investigated the development of the elliptical hole pattern in compressed monoholar metamaterials. We simulated the first unstable mode of monoholar samples under compression, and showed how the hole pattern forms and evolves. We showed different patches of the hole pattern which is affected by the parity of the number of holes, and in particular, we studied the snapping action caused by the frustration between two patches. Finally, we broke the symmetry of experimental samples by defect holes, and showed how the evolution of the hole pattern can be tuned by such geometric defects.